Taylor & Francis
Taylor & Francis Group

RESEARCH ARTICLE

OPEN ACCESS | Check for updates

Cell penetrating peptides functionalized gambogic acid-nanostructured lipid carrier for cancer treatment

Rui Huang[a,b], Jiawei Li[a,b], Dereje Kebebe[a,b,c], Yumei Wu[a,b], Bing Zhang[a,b] and Zhidong Liu[a,b]

[a]Tianjin State Key Laboratory of Modern Chinese Medicine, Institute of Traditional Chinese Medicine, Tianjin University of Traditional Chinese Medicine, Tianjin, P.R. China; [b]Engineering Research Center of Modern Chinese Medicine Discovery and Preparation Technique, Ministry of Education, Tianjin University of Traditional Chinese Medicine, Tianjin, P.R. China; [c]School of Pharmacy, Institute of Health Sciences, Jimma University, Jimma, Ethiopia

ABSTRACT

Tumor-targeted delivery is considered a crucial component of current anticancer drug development and is the best approach to increase the efficacy and reduce the toxicity. Nanomedicine, particularly ligand-based nanoparticles have shown a great potential for active targeting of tumor. Cell penetrating peptide is one of the promising ligands in a targeted cancer therapy. In this study, the gambogic acid-loaded nanostructured lipid carrier (GA-NLC) was modified with two kinds of cell penetrating peptides (cRGD and RGERPPR). The GA-NLC was prepared by emulsification and solvent evaporation method and coupled with cRGD, RGERPPR, and combination cRGD and RGERPPR to form GA-NLC-cRGD, GA-NLC-RGE, and GA-NLC-cRGD/RGE, respectively. The formulations were characterized by their particle size and morphology, zeta potential, encapsulation efficiency, and differential scanning calorimetry. In vitro cytotoxicity and cellular uptake study of the formulations were performed against breast cancer cell (MDA-MB-231). Furthermore, in vivo biodistribution and antitumor activity of the formulations were determined by in vivo imaging and in tumor-bearing nude mice, respectively. The result of in vitro cytotoxicity study showed that GA-NLC-RGE exhibited a significantly higher cytotoxicity on MDA-MB-231 as compared with GA-NLC and GA-Sol. Similarly, RGE-Cou-6-NLC showed remarkably higher uptake by the cells than other NLCs over the incubation period. The in vivo imaging study has demonstrated that among the formulations, the RGE-decorated DiR-NLC were more accumulated in the tumor site. The in vivo antitumor activity revealed that RGE-GA-NLC inhibits the tumor growth more efficiently than other formulations. In conclusion, RGERPPR has a potential as an effective carrier in targeting drug delivery of anticancer agents.

1. Introduction

Despite the rapid development of chemotherapeutic drugs over the past decades, cancer remains among the deadliest of human diseases in the world. Currently, clinically used drugs in chemotherapy are based on cytotoxic compounds that primarily inhibit the fast proliferation of the cancer cells, but unfortunately, they also inhibit the rapidly growing cells that are needed for the maintenance of hair follicles, bone marrow and gastrointestinal tract cells which leads to the undesirable side effects observed in cancer treatment (Chabner & Roberts, 2005). The traditional Chinese medicine has attracted the researchers' attention with the emerging of paclitaxel, camptothecin, vincaleukoblastinum, which have been widely considered as less toxic and effective antitumor effect. Gambogic acid (GA) is a small molecule extracted from the traditional Chinese medicine gamboges, which has been used for hundreds of years in China. Both in vitro and in vivo studies have demonstrated that GA exhibited potent anticancer activity in numerous types of human cancer cells, including prostate, gastric carcinoma, hepatocarcinoma, lung cancer, and breast carcinoma cells (Yang et al., 2007; Qi et al., 2008; Gu et al., 2009) and it has been approved for phase II clinical trials by the Chinese Food and Drug Administration (Gu et al., 2008; Chi et al., 2013). The unique caged xanthone structure which has multiple targets, including the Bcl-2 family proteins, redox regulatory protein, NF-κB and integrin pathways, was the basis of antitumor activity of GA (Zhang et al., 2004; Pandey et al., 2007). Hence, GA could influence several critical signaling pathways to induce multiple anticancer effects, involving the induction of apoptosis, the inhibition of proliferation and the prevention of cancer metastasis and tumor angiogenesis (Wang & Chen, 2012). Most of all, is that GA displays potent cytotoxicity toward carcinoma cells selectively, and has no toxic effect on hemameba and normal hematopoietic system (Yang et al., 2007). However, the poor aqueous solubility (<1 μg/mL), short half-

life (<1 h in dogs and <20 min in rats) and obvious topical venous stimulation preclude the clinical application of GA (Liu et al., 2006; Hao et al., 2007; Zhang et al., 2013). Therefore, drug carrier designs such as polymeric micelles and magnetic Fe_3O_4 nanoparticles (Zhu et al., 2008; Wang et al., 2012; Yu et al., 2013) have been investigated to improve the solubility and inhibitory effect of GA in tumor cells.

Considering that GA is inclined to induce the carcinoma cells apoptosis selectively (Yang et al., 2007), it is crucial to focus on drug concentrations accumulated in the tumor tissue, because the tumor microenvironment is significantly different from normal tissues. Nanoparticles can pass through abnormally large gaps (up to 1.5 μm) between endothelial cells that compose the leaky tumor vasculature and accumulate within the tumor (Setyawati et al., 2015). The phenomenon whereby nanoparticles accumulate in the tumor due to the leakiness of the vasculature is referred to as the enhanced permeability and retention (EPR) effect (Pérez-Herrero & Fernández-Medarde, 2015). The nanostructured lipid carriers (NLCs), which are mixtures of solid and liquid lipids, have been concerned on account of the fantastic biocompatibility, the long resident time in blood and passive targeting to tumors owing to nanoscale particle size (Attama, 2011; Selvamuthukumar & Velmurugan, 2011). It is reported that (Williams et al., 2013) the liquid lipid can embed into solid lipid matrix or localize at the interface of the solid matrix and the surfactant layer. These spatially different lipids lead to generally imperfectible crystal structure thus provide more space for accommodating the encapsulated drugs, as a consequence, NLCs were characterized by higher drug incorporation rate and better stabilization (Uner, 2006). In addition, NLC exhibit excellent biocompatibility compared with polymer-based nanocarriers. Furthermore, in contrast to liposomes, NLC is less costly and easier to scale up their production (Fang et al., 2015; Poonia et al., 2016).

Active targeting of tumor is achieved by attaching specific ligands to the nanoparticle structure, allowing a selective recognition of different receptors or antigens overexpressed in the tumor cell surfaces, increasing the cytotoxicity of the anticancer agents in tumors and avoiding most of their side effects, since the exposure of healthy cells to the drug is minimized (Steichen et al., 2013). One of the most efficient ways is to choose the ligands that target multiple cell types composing a tumor involves proliferation inhibition and anti-angiogenesis. αvβ3-Integrins are the most promising therapeutic target because they are overexpressed on the actively proliferating endothelium of tumor tissues and are determinants on angiogenic endothelium (Hynes, 2002; Jin & Varner 2004; Dubey et al., 2011).

The cyclic arginine-glycine-aspartate (cRGD) peptide has shown a strong binding affinity toward αvβ3-integrin overexpressed in angiogenic endothelial cells and several malignant cancer cells such as glioblastoma and melanoma (Graf et al., 2012; Miura et al., 2013; Zhong et al., 2014; Chen et al., 2015; Shi et al., 2015; Guo et al., 2016).

Neuropilin-1 (NRP1) is a transmembrane glycoprotein that acts as a co-receptor for a number of extracellular ligands including class III/IV semaphorins, certain isoforms of vascular endothelial growth factor and transforming growth factor beta (Chaudhary et al., 2014). In addition, cell-penetrating peptides (CPPs) which express a C-terminal consensus R/KXXR/K sequence interact with the b1/b2-domain of NRP1 inducing internalization of the CPPs into NRP1-expressing cells via an endocytic 'bulk transport' mechanism (Chaudhary et al., 2014). Theoretically, CPPs can be combined with therapeutic agents for selective tissue penetration and improved delivery. Recently, there has been a great deal of interest in NRP1 as a mediator of tumor development and progression since it was observed to be extensively expressed in tumor vasculature, where NRP1 over expression is associated with tumor progression and poor clinical outcome (Prud'homme & Glinka, 2012). A novel small-peptide RGERPPR obtained by the phage display screening, similar to the configuration of VEGF-A, was shown to have a high affinity toward NRP1-over-expressed cancer cells and tumor vasculature endothelial cells inducing effective tumor infiltration, making it a promising candidate for tumor-targeted therapy.

Accordingly, it could be hypothesized that the co-expression receptors of tumor tissue could be exploited to enhance tumor penetration of chemotherapeutic drugs. In this study, we designed the linear-peptide RGERPPR (RGE) and cyclic-peptide CRGDRGPDC (cRGD) functionalized NLCs for tumor-targeted delivery. Then, we compare the affinity of NLC conjugated with the RGERPPR, cRGD, and combination of them by their cytotoxicity (% cell viability) against three tumor cell lines which are human breast cancer MDA-MB-231 cells, human lung carcinoma Calu-3 cells, and mouse breast cancer 4T1 cells. However, the MDA-MB-231 cells were selected for further investigation of the targeting efficiency of different nanoparticles via cellular uptake assay. Subsequently, the models of nude mice bearing tumor were established by subcutaneous injection of MDA-MB-231 tumor cells on the right side of axillary. In vivo imaging and in vivo anti-tumor effect were evaluated in MDA-MB-231 xenografts, extensively.

2. Materials and methods

2.1. Materials

GA with a purity of more than 98% was purchased from Sichuan Weikeqi Bio-Tech Co. Ltd (Chengdu, China). RGERPPR and CRGDRGPDC peptides (Supplementary Figure S1) were synthesized by Chinapeptide Biotech Co. Ltd. (Shanghai, China). DSPE–PEG2000–NHS was purchased from Shanghai Advanced Vehicle Technology Pharmaceutical Co. Ltd. (Shanghai, China). N-(3-Dimethylaminopropyl)-N-ethylcarbodiimide (EDC) was provided by Civi Chemical Technology Co Ltd (Shanghai, China). Coumarin-6 was purchased from Sigma (Saint Louis, MO). 1,10-Dioctadecyl-3,3,3,3-tetramethyl indotricarbocyanine iodide (DiR), near-IR lipophilic carbocyanine dye, was obtained from Biotium Inc. (Hayward, CA). Paraformaldehyde (4%) was obtained from Solarbio Science and Technology Co Ltd (Beijing, China). 4,6-Diamidino-2-phenylindole (DAPI) was purchased from Beyotime (Haimen, China). 0.25% Trypsin–EDTA (1×), penicillin (10,000 units/mL) and streptomycin (10,000 μg/mL) were purchased from Life Technologies. Cell Counting Kit 8 (CCK-8) was obtained from

Dojindo Laboratories (Kumamoto, Japan). All the other chemicals were analytical reagent grades and purchased from Tianjin Guangfu Fine Chemical Research Institute (Tianjin, China).

Human breast carcinoma MDA-MB-231 cells were obtained from ATCC (Manassas, VA) and were cultivated in L-15 medium (Corning) added to 10% fetal bovine serum (Gibco), 100 units/mL penicillin, and 100 mg/mL streptomycin at 37 °C in a humidified atmosphere containing 5% CO_2. Human lung adenocarcinoma Calu-3 cells were obtained from ATCC (Manassas, VA) and cultivated in complete growth medium consisting of 89% IMDM (Gibco), 10% FBS (Gibco) and 1% penicillin–streptomycin. Mice breast cancer 4T1 cells were obtained from ATCC (Manassas, VA) and cultivated in 1640 medium (89%, Corning) including 10% FBS and 1% penicillin–streptomycin.

BALB/c nude mice (female, 4–5 weeks, 18–22 g) were obtained from the Institute of Radiation Medicine Chinese Academy of Medical Sciences (Tianjin, China) and housed at 25 ± 1 °C with access to food and water ad libitum in a specific pathogen-free (SPF) environment. All animal experiments were carried out in accordance with protocols evaluated and approved by the ethics committee of Tianjin University of Traditional Chinese Medicine.

2.2. Preparation of NLC

GA-loaded unconjugated NLC (GA-NLC) were prepared by emulsification and solvent evaporation method (Liu et al., 2015). Briefly, GA and lecithin were dissolved in ethanol, and ATO888 and MCT812 were dissolved in chloroform, mixed them together to get oil phase in the organic solvent. The aqueous phase was prepared by dissolving the prescribed quantity of Myrj 52 in deionized water. The oil phase was quickly added into the aqueous phase under magnetic stirring at 75 °C. The nanoemulsion was kept under stirring for 2 h to evaporate organic solvent and solidified in the refrigerator at 4 °C followed by characterization for size, zeta potential, morphology, encapsulation efficiency, and differential scanning calorimetry (DSC).

For the preparation of RGERPPR and CRGDRGPDC modified GA-NLC, the DSPE–PEG2000–NHS was dissolved in chloroform, and the other steps were according to the procedure mentioned above for NLC. The amino group of RGERPPR and CRGDRGPDC were further coupled to the NHS group of DSPE–PEG2000–NHS on the surface of nanoparticles via the maleimide-amino reaction. In detail, the solution of RGERPPR (2 mg/mL) and CRGDRGPDC (3 mg/mL) in phosphate buffer (pH 7.4) were added in a drop-wise manner to nanoparticles solution which was pre-incubated with EDC for 0.5 h, and the resulting mixture was kept under gentle stirring in the dark for 15 h at ambient temperature. After then, the dispersion was purified using a Hitrap desalting column to remove the unconjugated peptides. Ultimately, the eluent was concentrated to obtain the final conjugate.

2.3. Characterization of NLC

2.3.1. Particle size, zeta potential, and morphology
Particle size and zeta potential of GA-NLC, GA-NLC-RGE and GA-NLC-cRGD, GA-NLC-RGE/cRGD were measured by photon correlation spectroscopy using Zetasizer, Nano ZS (Malvern Instruments, Malvern, UK). Furthermore, transmission electron microscope (TEM; JEOL Ltd., Tokyo, Japan) was used to evaluate the surface morphology of the GA-NLC and modified GA-NLC.

2.3.2. Entrapment efficiency
Entrapment efficiency was determined by measuring the concentration of unloaded drug in dispersion collected after centrifugation of nanoparticle dispersion at 4000 r/min and 4 °C, for 20 min, and analysis was conducted using the validated high-performance liquid chromatography (HPLC) methods

2.3.3. HPLC method
2.3.3.1. Chromatographic condition.
The GA content was determined by the HPLC system with the ultraviolet detector (Shimadzu Corporation, Kyoto, Japan) and an octadecylsilane column (Inertsil, 250×4.6 mm, 5 mm) maintained at 30 °C. The mobile phase consisted of methanol and 0.1% phosphoric acid water (95:5), was pumped at a flow rate of 1.0 mL/min and monitored at a wavelength of 360 nm.

2.3.3.2. Preparation of standard curve.
Accurately, 5 mg of standard GA was weighed and dissolved in 50 mL methanol to make the stock solution of GA (100 µg/mL). The appropriate amount of GA stock solution was diluted with methanol to 2, 4, 6, 12 and 20 µg/mL, respectively. The calibration curves of the peak area (A) versus the concentration (C) were constructed.

2.3.3.3. Precision and accuracy.
Intra-day precision was determined by repeated analysis of sample (2, 4 and 12 µg/mL) on one day ($n = 5$), and inter-day precision was determined by repeated analysis on three consecutive days. The precision was expressed as the inter-day and intraday relative standard deviation [RSD = (SD/mean) $\times$ 100%]. The lower, medium, higher concentration of GA (2.008, 6.024 and 12.048 µg/mL, respectively) were used to determine the accuracy.

2.3.4. Differential scanning calorimetry
The physical state of GA inside the final formulation (GA-NLC) was investigated by DSC. DSC measurements were carried out on the samples: (a) GA, (b) physical mixture of Blank-NLC and GA, (c) GA-NLC, and (d) Blank-NLC. DSC studies were performed in a (DSC822e, Mettler Toledo GmbH, Greifensee, Switzerland), using aluminum open pans. The heating rate was 10 °C/min, with a temperature range of 30–250 °C and a 50 mL/min nitrogen flow.

2.4. Cytotoxicity assay

The cytotoxicity of different formulations was evaluated by CCK-8 kit. Three cell lines, MDA-MB-231 cells, 4T1 cells and Calu-3 cells were selected as the objects for the study. Cells in the logarithmic growth phase were seeded in 96-well plates at a density of 2×10^4 cells/mL. Twenty-four hours later, different GA formulations were added with a serial concentrations (10–0.25 μg/mL) which were prepared with sterile basal medium. Twenty-four hours later, the medium containing drugs was removed by pipettor and the cells were washed three times with PBS. Hundred microliter of 10% CCK-8 dilution was then added into each well, after incubation for 1 h at 37 °C, the absorbance at 450 nm wavelength was read by a multifunctional microplate reader (Multiskan MK3; Thermo Scientific, Atlanta, GA). Cell viability (%) was calculated by the following formula.

$$\text{Cell vialbility } (\%) = \frac{A_s - A_b}{A_C - A_b} \times 100$$

where, A_s, A_c and A_b refer to the absorbance of the experimental wells, the control wells, and the blank wells, respectively

2.5. Cellular uptake

MDA-MB-231 cells in the logarithmic growth phase were seeded in 96-wells plate at a density of 1×10^4 cells/mL. Twenty-four hours later, 0.002 μg/mL of coumarin-6-loaded NLC (Cou-6-NLC, Cou-6-NLC-RGE, Cou-6-NLC-cRGD, Cou-6-NLC-RGE/cRGD) and Cou-6-solution were added into the wells and incubated with cells at 37 °C, 5% CO_2 condition for 0.5, 2, 4 and 12 h, respectively. The adsorptive and free particles were removed by washing with ice-cold PBS three times. The cells were fixed with 4% paraformaldehyde for 20 min and the nuclei were stained by 0.20 μg/mL of DAPI solution to locate the cells for 10 min. Then, subsequently the cellular internalization of coumarin-6 was analyzed by High Content Cell Imaging Analysis System (GE InCell Analyzer 2000, Fairfield, CT).

2.6. In vivo imaging

Tumor-bearing mice were established as described previously (Miura et al., 2013). Briefly, ~1×10^7 MDA-MB-231 cells were subcutaneously injected in the scapular region of the mice. Tumors were allowed to grow to an average volume of ~50 mm³ in diameter before the experiment. The fluorescent dye DiR was entrapped into the NLC to investigate the tumor-targeting efficacy of different formulations of NLC *in vivo*. DiR-NLC, DiR-cRGD-NLC, DiR-RGE-NLC and DiR-cRGD/RGE-NLC were injected into tumor-bearing mice via the tail vein at a DiR concentration of 25 μg/mL, respectively. At 1, 2, 4, 8, and 24 h post-injection, the mice were anesthetized, and whole-body fluorescence images were acquired using a near-infrared fluorescence imaging system (Kodak, Rochester, NY) with a wavelength set at Ex =748 nm, Em =780 nm. During the imaging acquiring process, 3% isoflurane anesthesia (Abbott laboratories, Chicago, IL) was administered to the

mice via a nose cone system. The fluorescence intensity of DiR at the tumor site was measured by using the region of interest (ROI) function and data are presented as mean ± SD (*n* = 3).

2.7. In vivo anti-tumor effect

Ten days after the cell injection, the nude mice whose xenografts reached a volume of 100 mm³ were randomly divided into seven groups (8 mice per group): saline group, GA solution group, GA-NLC group, GA-NLC-RGE group, GA-NLC-cRGD group, GA-NLC-RGE/cRGD group and cisplatin group; each mouse was injected intravenously via the tail vein with the above formulations at a dose of 5 mg/kg every 2 days for seven times, meanwhile the weight and tumor volume was recorded before every injection. The tumor sizes were measured by calipers and the volume was calculated according to the formula $V = 0.5 \times L \times W^2$, wherein L is the tumor dimension at the longest point, W is the tumor dimension at the widest point. The tumor volume growth and weight change were graphed to reveal the trends. Mice were sacrificed three days afterward the last injection, the tumors were weighed, and the inhibition ratio (IR) was calculated as follows: IR (%) = $[(x−y)/x] \times 100\%$, where x and y represent the average tumor weight for the control group and treatment group, respectively.

2.8. Statistical analysis

The quantitative data were presented as mean ± standard deviation (SD). Statistical significance was analyzed using Student's *t*-test with the *p* value <0.05 indicating significance.

3. Results and discussion

3.1. Characterization of NLC

The particle size of GA-NLC, GA-NLC-RGE, GA-NLC-cRGD and GA-NLC-RGE/cRGD were found in the range of 20–25 nm with a zeta potential of approximately from −2 to −6 mV (Table 1 and Supplementary Figure S2). The particles were generally spherical in shape as confirmed by TEM (Supplementary Figure S3).

3.2. Differential scanning calorimetry

According to the DSC study, the melting endothermic peak of pure GA appeared at 173 °C. However, no melting peak was detected for GA-NLC (Supplementary Figure S4).

Table 1. Particle size, polydispersity index, zeta potential and entrapment efficiency of GA-NLC and CPP-modified GA-NLC.

Groups	Particle size (nm)	PDI	Zeta potential (mV)	Entrapment efficiency (%)
GA-NLC	20.96 ± 1.13	0.23 ± 0.08	−5.86 ± 0.64	99.46 ± 0.43
GA-NLC-RGE	22.13 ± 0.79	0.19 ± 0.04	−3.50 ± 2.01	
GA-NLC-cRGD	21.01 ± 0.54	0.20 ± 0.09	−4.01 ± 0.67	
GA-NLC-RGE/cRGD	25.81 ± 0.66	0.24 ± 0.06	−1.98 ± 1.01	

GA: gambogic acid; NLC: nanostructured lipid carrier; CPP: cell penetrating peptide.

The probable reason could be that GA has completely solubilized in the lipid matrix or change in crystallinity (Padhye & Nagarsenker, 2013).

3.3. HPLC method validation

The calibration curve showed a good linearity over concentration ranges (2.008–20.08 μg/mL) with correlation coefficient (r^2) of 0.9995 and the standard curve equation is $A = 13668C - 4372.4$. The accuracy of low, medium and high concentrations was found to be 95.62, 104.26 and 96.60%, respectively. The intra-day RSD of low, medium and high concentrations of GA solution was 1.2, 0.5 and 0.6%, respectively. The inter-day RSD was 1.9, 1.9 and 1.3%, respectively, which were <2%, indicating that the method is precise, accurate and reliable for the determination of content of GA.

3.4. Cytotoxicity

The cytotoxicity of the conjugated and unconjugated formulation was evaluated in MDA-MB-231, 4T1, and Calu-3 cell lines. The cell viability was found to decrease with the increase in the drug concentration. A quantitative evaluation of *in vitro* therapeutic effect of a dosage form is IC_{50}, which is the drug concentration needed to kill 50% of the incubated cells in a designated time. It can be calculated from the *in vitro* cellular viability data after the treatment. Accordingly, the IC_{50} was 0.41, 0.30 and 0.09 μg/mL for free GA, GA-NLC, and GA-NLC-RGE formulation in MDA-MB-231 cell lines, respectively (Figure 1). In 4T1 cells, whereas, there was two-fold differences in IC_{50} of GA-NLC as compared to GA-Sol. IC_{50} was found to be 0.44 μg/mL for free GA, 0.39 μg/mL for GA-NLC and 0.22 μg/mL for GA-NLC-RGE. A significantly higher cytotoxicity ($p < .05$) or lower IC_{50} of GA-NLC-RGE formulation in both cell lines indicate that conjugating RGERPPR on the surface of NLC increases the targeting efficiency of GA in mentioned cells, caused by the enhanced endocytosis mediated by the Neuropilin-1 receptors. The significant increase in toxicity of GA-NLC compared to GA-Sol

can be attributed to the passive targeting of nanoparticles. Hence, these studies justified the use of RGERPPR as targeting ligand to target tumors over expressing NRP1 receptors.

3.5. Cellular uptake

Targeting effect of RGERPPR and cRGD decorated lipidic nanoparticles can be evaluated by investigating their cellular uptake. The cellular uptakes of the lipidic formulations were qualitatively and quantitatively evaluated by using coumarin-6 (instead of GA) incorporated NLC, NLC-RGE, NLC-cRGD and NLC-RGE/cRGD and employing High Content Cell Imaging Analysis System to measure the intracellular fluorescence intensity. The conjugated NLC-RGE, NLC-cRGD, and NLC-RGE/cRGD formulation showed higher uptake than unconjugated NLC formulation as shown in the fluorescent images of MDA-MB-231 cell lines after incubation for 0.5, 2, 4, and 12 h (Figure 2). Intracellular quantitative fluorescence intensity of coumarin-6-Sol, coumarin-6-NLC, coumarin-6-NLC-RGE, coumarin-6-NLC-cRGD, coumarin-6-NLC-RGE/cRGD after incubation in MDA-MB-231 for 12 h were found to be 8.61 ± 4.47, 192.4 ± 58.91, 342.34 ± 51.75, 254.4 ± 93.19, and 245.8 ± 108.8, respectively (Figure 2). As a control, negligible fluorescence inside MDA-MB-231 cells was observed after incubating with the coumarin-6 solution, which clearly indicates the uptake of RGERPPR coupled NLC via the NRP1 receptors which are expressed on the cancer cells currently studied. This study also confirmed that the higher cytotoxicity of coumarin-6-NLC-RGE as found from CCK-8 cell viability assay. RGERPPR could significantly enhance the MDA-MB-231 cells uptake of the formulations. This could be owed to the high vascular permeability of RGERPPR in the tumor in MDA-MB-231.

3.6. In vivo *and* ex vivo *imaging*

The tumor-targeting abilities of NLC, NLC-RGE, NLC-cRGD and NLC-RGE/cRGD were assessed in the MDA-MB-231 breast tumor xenograft mouse model using DiR. DiR was selected
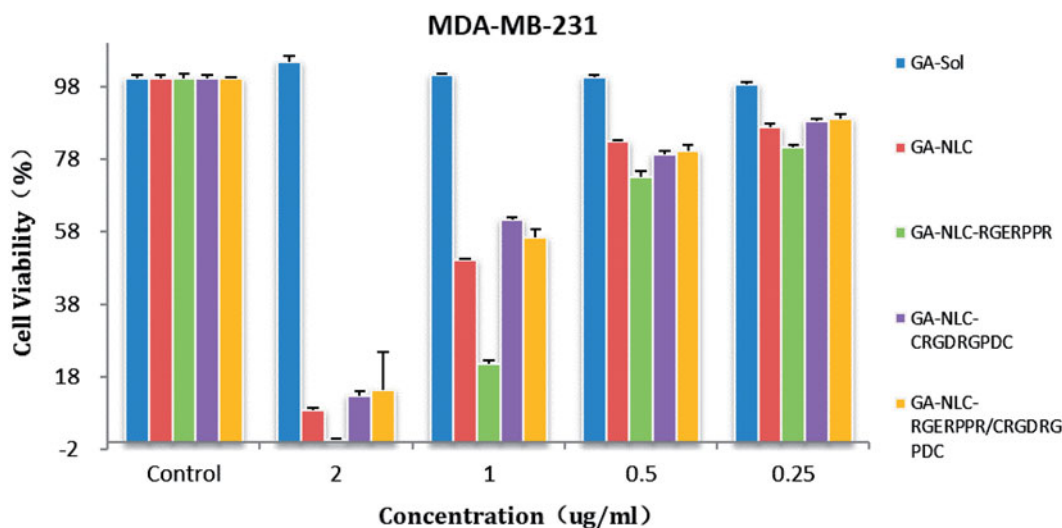

Figure 1. Cytotoxicity of GA-sol, GA-NLC, and peptide-modified GA-NLC in MDA-MB-231 cell.
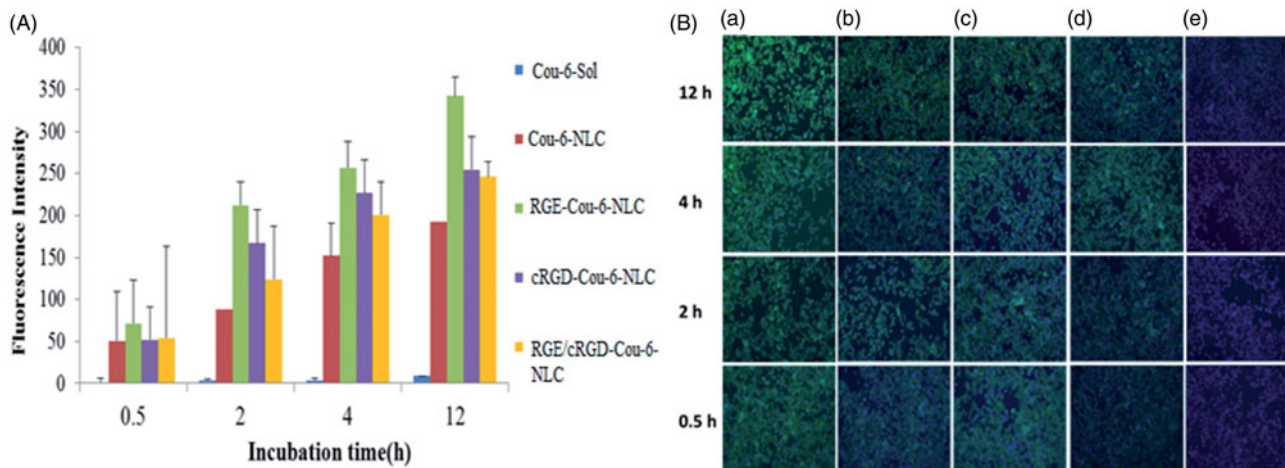
Figure 2. (A) Fluorescence intensity of different Cou6-loaded formulation in MDA-MB-231 cells. (B) Cellular uptake of Cou-6 formulations at different time intervals. a: Cou-6-NLC-RGE, b: Cou-6-NLC-cRGD, c: Cou-6-NLC-RGE/cRGD, d: Cou-6-NLC and e: Cou-6-Sol.
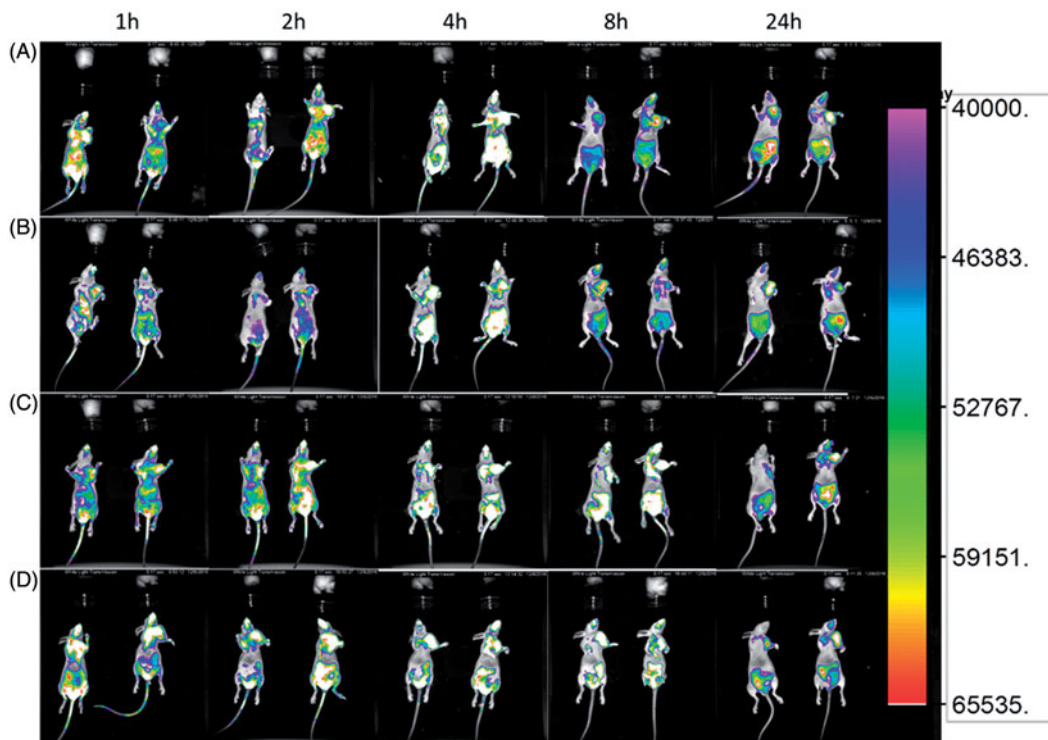

Figure 3. The *in vivo* imaging of the nude mouse after administration of DiR-loaded formulations. A: DiR-NLC-RGE, B: DiR-NLC-cRGD, C: DiR-NLC-RGE/cRGD, D: DiR-NLC.

as the fluorescent probe in this study because of its NIR excitation and emission wavelength, which could effectively reduce the interference of animal auto-fluorescence (Sharma et al., 2006). Time-dependent biodistribution of DiR-NLC and peptides-modified DiR-NLC was visualized after intravenous administration using a noninvasive NIR imaging technique. As represented in Figure 3, DiR-NLC-RGE exhibited the strongest fluorescence signal at the tumor site as compared with other groups. Moreover, the fluorescence detected in DiR-NLC group faded away rapidly, while it was sustained at the tumor location in DiR-NLC-RGE group at all the time points of postinjection. These observations suggest a tumor-specific accumulation of the NLC, particularly DiR-NLC-RGE.

Twenty-four hours post-administration, *ex vivo* imaging was performed (Supplementary Figure S5). The fluorescent images of the excised tumors and major organs of the sacrificed mice showed that DiR-NLC-RGE was accumulated in tumors more efficiently than the other groups, suggesting an enhanced tumor-specific targeting ability of the RGE. The lowest fluorescent signal in the tumor was detected in DiR-NLC group, and the accumulation of DiR-NLC group in livers and spleen was higher than in other organs. The semiquantitative analysis of the fluorescent images was in good agreement with *ex vivo* imaging results. DiR-NLC-RGE showed over 1.9-fold higher fluorescence intensity at the tumor than unconjugated NLC-DiR.
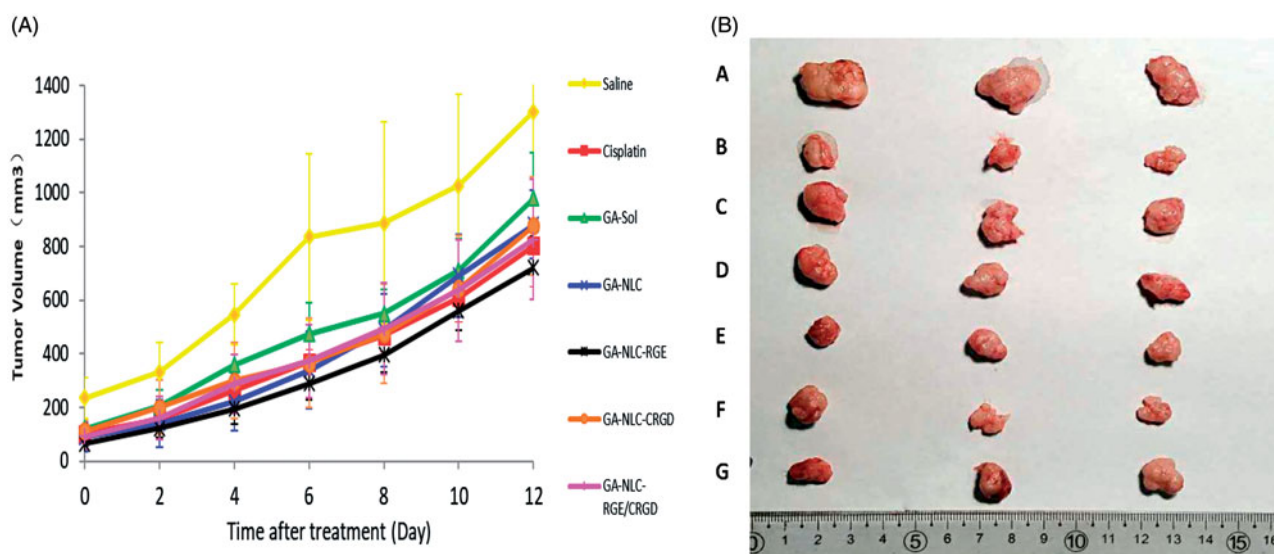
Figure 4. (A) Change in the volume of tumor over the course of treatment. (B) The volume of excised tumor tissue. A: Saline, B: cisplatin, C: GA-Sol, D: GA-NLC, E: GA-NLC-RGE, F: GA-NLC-cRGD and G: GA-NLC-RGE/cRGD.
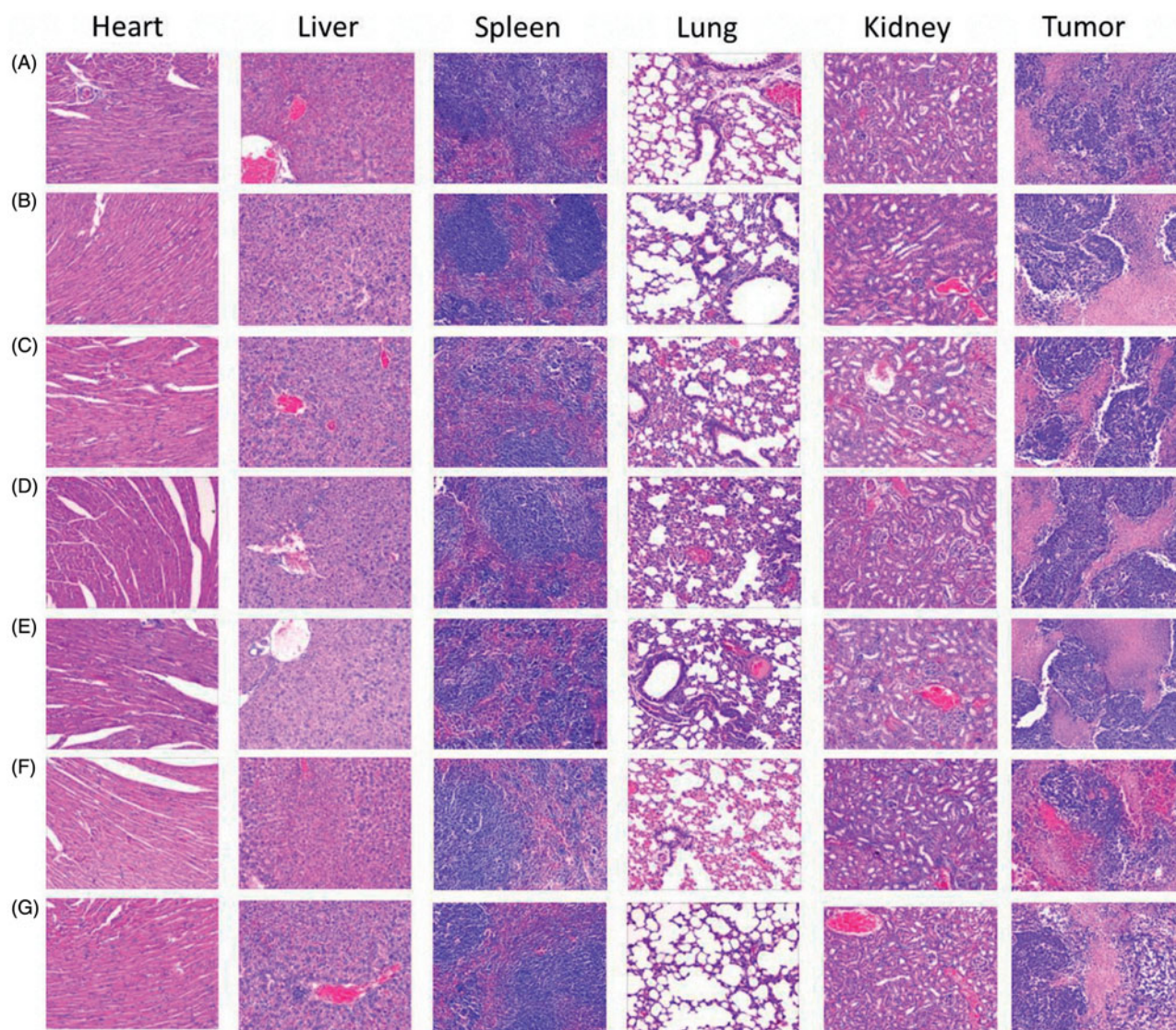

Figure 5. HE staining of major organs and tumor tissue. (A) Saline, (B) cisplatin, (C) GA-Sol, (D) GA-NLC, (E) GA-NLC-RGE, (F) GA-NLC-cRGD and (G) GA-NLC-RGE/cRGD.

3.7. Anti-tumor effect

To provide *in vivo* evidence for the antitumor potential of CPP-modified GA-NLC, the antitumor efficacy was evaluated using an MDA-MB-231 tumor-bearing mouse model. As shown in Figure 4, compared to the saline solution group (negative control), the six treatment groups showed distinct tumor growth inhibition efficiency. Specifically, the group treated with free GA, GA-NLC, GA-NLC-RGE, GA-NLC-cRGD, GA-NLC-RGE/cRGD and Cisplatin (positive control), showed smaller tumor volumes than the saline control group ($p < .05$). Moreover, GA-NLC-RGE displayed a marked reduction in tumor size, when compared with other groups. The final tumor weight is shown in Figure 4(B), and was in good agreement with tumor volume assay. The results revealed that GA-NLC-RGE inhibited the tumor growth most efficiently and the IR calculated from tumor weight was 83.3%; and followed by Cisplatin (73.33%), GA-NLC-cRGD (66.67%), GA-NLC-RGE/cRGD (65.00%), and free GA (45%). The body weight investigation was applied to evaluate systemic toxicity in mice. Compared with the saline group, the mice in free GA group showed a significant decrease in body weight, while no notable change was found in GA-NLC-RGE groups.

3.8. HE staining

The microscopic changes of organs were characterized histologically to evaluate the toxicity of different formulations. As shown in Figure 5, there were no differences among the formulations in resulting considerable microscopic changes on major organs. No noticeable sign of damage was observed in lung, spleen, kidney, heart, and liver, suggesting the formulations could not cause obviously systemic toxicity. The metronomic therapy that was used in this study (5 mg/kg every 2 days for seven times) displayed a lower toxicity than maximum-tolerated dose does, which could be one of the reasons for the different formulations showed the similar and low toxicity.

4. Conclusion

In this study, we have demonstrated that the novel nanocarrier based on CPP selectively target the breast tumor not only by EPR effect, but also through active dual-targeting endocytosis mechanism. Both *in vitro* and *in vivo* results confirmed their predominant effects in enhancing drug efficacy. Therefore, we can conclude that RGERPPR-modified NLC is supposed to be a promising and desirable vehicle for anticancer drugs like GA to treat breast cancer.

Disclosure statement

No potential conflict of interest was reported by the authors.

Funding

References

Attama AA. (2011). SLN, NLC, LDC: state of the art in drug and active delivery. Recent Pat Drug Deliv Formul 5:178–87.

Chabner B, Roberts T. (2005). Timeline: chemotherapy and the war on cancer. Nat Rev Cancer 5:65–72.

Chaudhary B, Khaled YS, Ammori BJ, et al. (2014). Neuropilin 1: function and therapeutic potential in cancer. Cancer Immunol Immunother 63:81–99.

Chen G, Wang L, Cordie T, et al. (2015). Multi-functional self-fluorescent unimolecular micelles for tumor-targeted drug delivery and bioimaging. Biomaterials 47:41–50.

Chi Y, Zhan XK, Yu H, et al. (2013). An open-labeled, randomized, multicenter phase IIa study of gambogic acid injection for advanced malignant tumors. Chin Med J 126:1642–6.

Dubey PK, Singodia D, Verma RK, et al. (2011). RGD modified albumin nanospheres for tumour vasculature targeting. J Pharm Pharmacol 63:33–40.

Fang G, Tang B, Chao Y, et al. (2015). Improved oral bioavailability of docetaxel by nanostructured lipid carriers: in vitro characteristics, in vivo evaluation and intestinal transport studies. RSC Adv 5:96437–47.

Graf N, Bielenberg DR, Kolishetti N. (2012). α(V)β(3) Integrin-targeted PLGA-PEG nanoparticles for enhanced anti-tumor efficacy of a Pt(IV) prodrug. ACS Nano 6:4530–9.

Gu H, Rao S, Zhao J, et al. (2009). Gambogic acid reduced bcl-2 expression via p53 in human breast MCF-7 cancer cells. J Cancer Res Clin Oncol 135:1777–82.

Gu H, Wang X, Rao S, et al. (2008). Gambogic acid mediates apoptosis as a p53 inducer through down-regulation of mdm2 in wild-type p53-expressing cancer cells. Mol Cancer Ther 32:3298–3305.

Guo Y, Niu B, Song Q, et al. (2016). RGD-decorated redox-responsive d-α-tocopherol polyethylene glycol succinate-poly (lactide)nanoparticles for targeted drug delivery. J Mater Chem B 4:2338–50.

Hao K, Liu XQ, Wang GJ, et al. (2007). Pharmacokinetics, tissue distribution and excretion of gambogic acid in rats. Eur J Drug Metab Pharmacokinet 32:63–8.

Hynes RO. (2002). A reevaluation of integrins as regulators of angiogenesis. Nat Med 8:918–21.

Jin H, Varner J. (2004). Integrins: roles in cancer development and as treatment targets. Br J Cancer 90:561–5.

Liu YT, Hao K, Liu X, et al. (2006). Metabolism and metabolic inhibition of gambogic acid in rat liver microsomes. Acta Pharmacol Sin 27:1253–8.

Liu Z, Zhao H, Shu L, et al. (2015). Preparation and evaluation of Baicalin-loaded cationic solid lipid nanoparticles conjugated with OX26 for improved delivery across the BBB. Drug Dev Industr Pharm 41:353–61.

Miura Y, Takenaka T, Toh K, et al. (2013). Cyclic RGD-linked polymeric micelles for targeted delivery of platinum anticancer drugs to glioblastoma through the blood-brain tumor barrier. ACS Nano 7:8583–92.

Padhye SG, Nagarsenker MS. (2013). Simvastatin solid lipid nanoparticles for oral delivery: formulation development and in vivo evaluation. Indian J Pharm Sci 75:591–8.

Pandey MK, Sung B, Ahn KS, et al. (2007). Gambogic acid, a novel ligand for transferrin receptor, potentiates TNF-induced apoptosis through modulation of the nuclear factor-kappaB signaling pathway. Blood 110:3517–25.

Pérez-Herrero E, Fernández-Medarde A. (2015). Advanced targeted therapies in cancer: drug nanocarriers, the future of chemotherapy. Eur J Pharm Biopharm 93:52–79.

Poonia N, Kharb R, Lather V, et al. (2016). Nanostructured lipid carriers: versatile oral delivery vehicle. Future Sci OA 2:FSO135.

Prud'homme G, Glinka Y. (2012). Neuropilins are multifunctional coreceptors involved in tumor initiation, growth, metastasis and immunity. Oncotarget 3:921–39.

Qi Q, Lu N, Wang X, et al. (2008). Anti-invasive effect of gambogic acid in MDA-MB-231 human breast carcinoma cells. Biochem Cell Biol 86:386–95.

Selvamuthukumar S, Velmurugan R. (2011). Nanostructured lipid carriers: a potential drug carrier for cancer chemotherapy. Lipids Health Dis 11:159.

Setyawati MI, Tay CY, Docter D, et al. (2015). Understanding and exploiting nanoparticles' intimacy with the blood vessel and blood. Chem Soc Rev 44:8174–99.

Sharma P, Brown S, Walter G, et al. (2006). Nanoparticles for bioimaging. Adv Colloid Interface Sci 123–126:471–85.

Shi KL, Cao J, Yang ZP, et al. (2015). A pH-responsive cell-penetrating peptide-modified liposomes with active recognizing of integrin αvβ3 for the treatment of melanoma. J Control Release 27:38–150.

Steichen SD, Caldorera-Moore M, Peppas NA. (2013). A review of current nanoparticle and targeting moieties for the delivery of cancer therapeutics. Eur J Pharm Sci 48:416–27.

Uner M. (2006). Preparation, characterization and physico-chemical properties of solid lipid nanoparticles (SLN) and nanostructured lipid carriers (NLC): their benefits as colloidal drug carrier systems. Int J Pharm Sci 61:375–86.

Wang X, Chen WT. (2012). Gambogic acid is a novel anti-cancer agent that inhibits cell proliferation, angiogenesis and metastasis. Anticancer Agents Med Chem 12:994–1000.

Wang CL, Zhang HJ, Chen Y, et al. (2012). Gambogic acid-loaded magnetic Fe(3)O(4) nanoparticles inhibit Panc-1 pancreatic cancer cell proliferation and migration by inactivating transcription factor ETS1. Int J Nanomed 7:781–7.

Williams HD, Trevaskis NL, Yeap YY. (2013). Lipid-based formulations and drug supersaturation: harnessing the unique benefits of the lipid digestion/absorption pathway. Pharm Res 30:2976–92.

Yang Y, Yang L, You QD, et al. (2007). Differential apoptotic induction of gambogic acid, a novel anticancer natural product, on hepatoma cells and normal hepatocytes. Cancer Lett 256:259–66.

Yu F, He C, Waddad AY, et al. (2013). N-Octyl-N-arginine-chitosan (OACS) micelles for gambogic acid oral delivery: preparation, characterization and its study on in situ intestinal perfusion. Drug Dev Ind Pharm 40:774–82.

Zhang HZ, Kasibhatla S, Wang Y, et al. (2004). Discovery, characterization and SAR of gambogic acid as a potent apoptosis inducer by a HTS assay. Bioorg Med Chem 12:309–17.

Zhang ZH, Wang XP, Ayman WY, et al. (2013). Studies on lactoferrin nanoparticles of gambogic acid for oral delivery. Drug Deliv 20:86–93.

Zhong Y, Meng F, Deng C, et al. (2014). Ligand-directed active tumor-targeting polymeric nanoparticles for cancer chemotherapy. Biomacromolecules 15:1955–69.

Zhu X, Zhang C, Wu XL, et al. (2008). Preparation, physical properties, and stability of gambogic acid loaded micelles based on chitosan derivatives. Drug Dev Ind Pharm 34:2–9.